RESEARCH ARTICLE

Force reveals hidden conformations and dissociation pathways in individual π-interacting dimers

Célia Franceschini, [a]‡ Dorothée Brandt, [b]‡ Maxime Ledent,[a] Thomas Carabin,[a] Hanna Traeger,[c,d] Jess M. Clough,[c,d] Luca Muccioli,[e] Anne-Sophie Duwez,[a] Christoph Weder,*[c,d] Yoann Olivier,*[b] Damien Sluysmans*[a]

[a] Célia Franceschini, Dr Maxime Ledent, Dr Thomas Carabin, Prof. Dr Anne-Sophie Duwez, Dr Damien Sluysmans
Research Unit MolSys, NanoChem
University of Liège
Allee du six août 14, 4000 Liège, Belgium
E-mail: Damien.Sluysmans@uliege.be

[b] Dorothée Brandt, Prof. Dr Yoann Olivier
Laboratory for Computational Modelling of Functional Materials, Namur Institute of Structured Matter
University of Namur, Belgium
E-mail: Yoann.Olivier@unamur.be

[c] Dr Hanna Traeger, Dr Jess M. Clough, Prof. Dr Christoph Weder
Adolphe Merkle Institute, University of Fribourg
Fribourg, Switzerland
E-mail: Christoph.Weder@unifr.ch

[d] Dr Hanna Traeger, Dr Jess M. Clough, Prof. Dr Christoph Weder
NCCR Bio-inspired Materials, University of Fribourg
Fribourg, Switzerland

[e] Prof. Dr Luca Muccioli
Department of Industrial Chemistry, University of Bologna
Bologna, Italy

‡ These authors contributed equally to the work

Abstract

Harnessing mechanical force to control molecular structure is a central strategy in the design of mechano-responsive materials. Noncovalent interactions are particularly attractive in this context because of their reversibility and tunable mechanical stability, yet the conformational energy landscapes of such motifs often remain inaccessible to conventional ensemble techniques. Here, we use atomic force microscopy-based force spectroscopy to probe individual π-interactions within a perylene diimide (PDI) dimer. Single-molecule pulling experiments combined with molecular dynamics simulations reveal two distinct long-lived conformers with *parallel* and *anti-parallel* PDI orientations that are indistinguishable by ensemble techniques. The *parallel* conformer exhibits greater mechanical stability and ruptures through a sequential pathway in which the dimer converts to an *anti-parallel* arrangement before π-π dissociation. Passive force spectroscopy resolves both conformers in real-time, validates the force-induced interconversion pathway predicted by steered molecular dynamics simulations, and quantifies their mechanical resistance and lifetime under constant load. Together, these results show that combining passive force spectroscopy with molecular simulations can reveal hidden conformational states in noncovalent assemblies and map their force-dependent energy landscape. Our findings provide molecular-level insight into the mechanics of π–π interactions and highlight single-molecule force spectroscopy as a powerful approach to uncover hidden structural states in supramolecular systems.

Introduction

By incorporating chemical interactions spanning a wide range of mechanical strengths, responsive polymers can be created that cover a broad range of macroscopic mechanical behaviors[1–8]. The integration of mechanophores, molecular motifs offering reactive chemical bonds that break or rearrange under load, has been shown to afford polymers whose macroscopic physico-chemical properties change in response to mechanical forces[9–14]. Unfortunately, the mechanical degradation of covalently linked chemical structures under high force is often accompanied by macroscopic degradation, which compromises these appealing properties. Other mechano-responsive polymer materials where the force-modulated units interact through mechanical bonds (*e.g.* catenated structures)[15–22] or noncovalent interactions (*e.g.* hydrogen bonds or π-stacks)[2,7,23–25] have been developed recently. The use of mechanical bonds attached to a polymer scaffold is very attractive due to the high precision and reproducibility of their response, but these motifs generally require considerable synthetic efforts. Noncovalent interactions offer a very attractive alternative due to their potential reversibility and high dynamic range. Their force-triggered rupture induces the dissociation of interacting partners or (macro)molecular conformational changes, therefore modifying the physico-chemical properties of the materials[26]. The reversible properties these interactions can support when integrated into macroscopic materials have attracted significant attention and led to the design of chemical architectures that incorporate them.[7] Following this approach, some of us introduced loop-forming perylene diimide (PDI) mechanophores and incorporated these motifs into polymers to act as macroscopically discernible fluorescent motifs under mechanical stress[23,27,28]. These mechanochromic materials integrate π-stacked PDI loops, a molecular design that offers an instantaneous and reversible fluorescence color change upon an external force. Other examples using noncovalent bonds within a rationally-designed architecture have been demonstrated recently, highlighting the importance of understanding the force-triggered response of weak chemical interactions[2,5,29–31].

The rational design of chemical structures adopting specific molecular conformations and desired mechano-chemical responses now requires a detailed molecular description, not accessible by typical ensemble physico-chemical characterizations techniques. Conversely, a precise picture of the force response, molecular conformational changes and force-induced mechanisms of a mechano-responsive molecular system can be drawn experimentally by single-molecule force spectroscopy (SMFS) techniques[32–37]. Atomic force microscopy (AFM)-based SMFS has been established as an efficient and cutting-edge approach to investigate the responses of individual molecules and interactions under controlled mechanical stress[33,35,38–40]. The chemical interactions in synthetic molecules probed by AFM range from covalent bonds[5,6,8,10,13,14,41] or coordination interactions[42–45] to very weak interactions or short-lived intermediates[46–54]. Although active force spectroscopy experiments, *i.e.* controlled molecular pulling under a force ramp, are by now an established approach to elucidate the effect of the force on an individual interaction, advanced passive SMFS experiments that depict the real-time behavior of a single bond held at a specific external force or extension are rare[10,54,55]. Here, we have taken advantage of the loop-forming motif reported earlier[23] and established experimental protocols to elucidate, in real time, the dynamics of individual π-interactions under force. Thus, the π-interactions between two perylene diimide (PDI) moieties were studied by active and passive single-molecule force spectroscopies. The latter technique allows us to probe and distinguish previously inaccessible conformational states. To support the experiments and provide a quantitative

interpretation of the conformational dynamics of the dimers and of their energetics, we complemented the analysis with simulations in an explicit solvent of a reduced mechanophore system consisting of one PDI dimer linked by a molecular bridge under mechanical stress.

Results and Discussion

Force rupture of an individual PDI dimer

We first performed active single-molecule pulling experiments in acetonitrile, on PDI dimers that were chemically modified for AFM measurements. Two perylene diimide units were bridged to form a small molecular loop[23] and polymer chains were grown from both PDI units to serve as an interface between a silicon substrate and the AFM tip (Fig. 1a). Poly(methyl acrylate) (PMA) blocks were employed as the flexible linkers, while poly(glycidyl acrylate) (PGA) segments were added to provide strong and time-resistant anchoring points, essential for passive SMFS measurements. The resulting macromolecular construct, integrating a single PDI dimer per chain, was purified and characterized by size-exclusion chromatography (SEC) and nuclear magnetic resonance (NMR) spectroscopy (details in SI). These macromolecules were grafted onto activated silicon substrates following established protocols[45,53], ensuring a very low grafting density to favour single-molecule attachment (details in SI).

In active SMFS experiments, the AFM tip is brought into contact with the grafted substrate to chemically attach a single macromolecule (*via* one or multiple PGA residues), which is then stretched during tip retraction (Fig. 1a). A characteristic force-extension (F-E) curve representing the mechanical stretching of an individual PDI dimer between two polymer linkers is shown in Fig. 1b. The low occurrence of molecular attachment with the tip (< 5% of all approaches) supports the typical low grafting density, in favor of single-molecule probing. The maximum extension of the stretched molecules (D_{rupt} < 250 nm, Fig. S4b) is consistent with the total length of the macromolecular construct. We measured the persistence length (l_p) of the linkers by applying a worm-like chain (WLC)[56] fitting on F-E curves before the first rupture point, revealing a l_p = 0.35 ± 0.12 nm (Fig. S4c) close to the monomer length, supporting that individual chains are probed. The unfolding of the PDI loop under load is evidenced by two subsequent rupture events (later referred to as *double-peak* profiles). Such specific profiles have been isolated from single-peak profiles corresponding to the stretching of a single polymer chain without any PDI dimer rupture. The distribution of extension variations (Δx) observed in the *double-peak* profiles is centred at 5.1 ± 1.9 nm (Fig. 1c). Perylene diimides are known to create π-π interactions in polar solvents due to their extended π-conjugated system, leading to a π-π distance of about 0.35 nm (*i.e.* distance between both PDI units in the folded form).[25,57] As confirmed also by our molecular mechanics model (*vide infra*), after the mechanical breaking of these interactions and alignment of the PDI units in the pulling direction, the distance between the PDI units reaches approximately 5.4 nm (total length of both PDI units and the bridging loop). The mechanical breaking of a single PDI-PDI interaction leads to a theoretically predicted extension of 5 nm, which matches the Δx measured in the SMFS experiment. Therefore, we hypothesize that the first peak observed in the force profile in Fig. 1b is associated with the rupture of π interactions between both PDI units, thus revealing the bridging loop, while the second one arises from the usual desorption of one polymer tether from the AFM tip or the substrate.

The mechanical strength of this π-interaction in acetonitrile is represented in Fig. 1d. The distribution of the PDI-PDI rupture force (first rupture, F_{peak}) presents two populations centered at 77 ± 17 pN (71 %) and 119 ± 16 pN (29 %), this force range being consistent with the breaking of donor-acceptor π-interactions previously reported[46,49,53]. No correlation of the rupture force populations with the revealed length distribution has been found, allowing us to exclude the attribution of the highest force population to the breaking of several PDI stacks in series[58,59]. Conversely, the observation of two force populations suggests the presence of two distinct folded conformations with different mechanical strengths, which are difficult to discriminate using typical active force spectroscopy experiments.

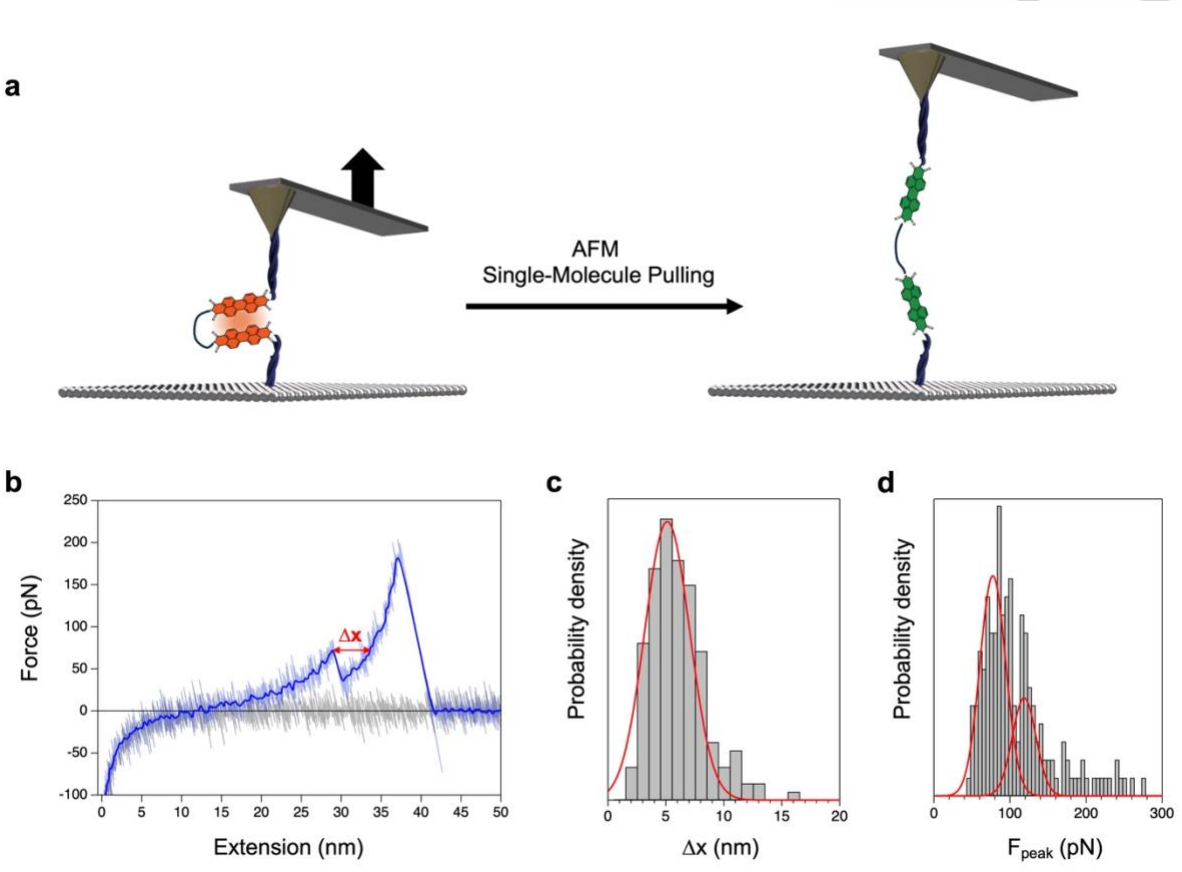

Figure 1. PDI dimers under active SMFS. (a) Schematic representation of a PDI dimer interfaced and stretched by AFM. The PDI folded conformation is stabilized by π-stacking interactions (represented in orange) that are mechanically broken during force spectroscopy experiments. A bridging loop (~5 nm) connects both PDI units. During the pulling experiment, the loop unfolds and eventually, PDIs are no longer π-stacked. (b) Force signature (in blue) of the mechanical PDI unfolding in acetonitrile showing a sudden force drop with a $\Delta x \approx 5$ nm (loop revealed); the final rupture event corresponds to the desorption of the polymer from the AFM tip or the substrate. The approach curve is represented in grey. (c) The distribution of the revealed length after the first rupture peak shows one population at $\Delta x = 5.1 \pm 1.9$ nm (N = 182), perfectly matching the length of the bridging loop. (d) The distribution of the PDI-PDI rupture forces exhibits two different populations at 77 ± 17 pN and 119 ± 16 pN (N = 182), representative of two distinct folded conformations.

Two distinct folded conformations of PDI dimers depicted by MD simulations

To elucidate the origin of these force populations, we considered a system where two PDIs are connected through a tetraethylene glycol–butanedione–tetraethylene glycol loop attached to one of their imide groups, while on the other imide group each PDI bears a tetraethylene glycol methyl ester pendant (Fig. 2a). We performed molecular dynamics simulations at room temperature and 1 atm (see SI for the detailed methodology) of this system solvated in acetonitrile, in which, starting from a fully extended bridging loop geometry, we observed the spontaneous formation of the PDI dimer (Movie S1).

The distribution of the cosine of the twist angle θ, *i.e*. the angle between the long axes of the two PDIs (inset in Fig. 2c, see Structural Analysis in SI) along the MD trajectory reveals a bimodal distribution. The two main conformations identified correspond to a more abundant *parallel* one (with $0 < \theta < 40°$), in which the imide groups connected by the linker are in proximity, and an *anti-parallel* one $(140 < \theta < 180°)$ in which the distance between them is larger (Fig. 2a and 2b). The bridging loop adopts a very different spatial arrangement in each folded conformation, surrounding the PDI dimer in the *anti-parallel* form while being away from the dimer in the *parallel* form. The spatial arrangement of the bridging loop can be quantified by introducing the bridge angle f (inset in Fig. 2d), with its vertex at the midpoint of the loop, and with the nitrogen atoms of the two PDI units defining its ends. The *anti-parallel* and *parallel* conformations have bridge angles ranging from 70 to 110° and 15 to 35°, respectively.

To explore the potential energy surface for the interconversion between the *parallel* and *anti-parallel* conformers, we carried out adaptive biasing force (ABF) simulations considering twist and bridge angles as collective variables. The resulting two-dimensional free energy map highlights a clear reaction pathway between the *parallel* and *anti-parallel* conformers, with a barrier of about 6 kcal·mol^{-1} between the two minima (Fig. 2e and SI for computational details). Interestingly, the transition between the *parallel* and *anti-parallel* conformations is entropically driven and proceeds through a maximum of entropy ($-T\Delta S$ minimum). The gain in conformational entropy lowers the free-energy barrier between the *parallel* and *anti-parallel* states (Fig. 2f), while the two conformers themselves remain enthalpically stabilized (Fig. S13b).

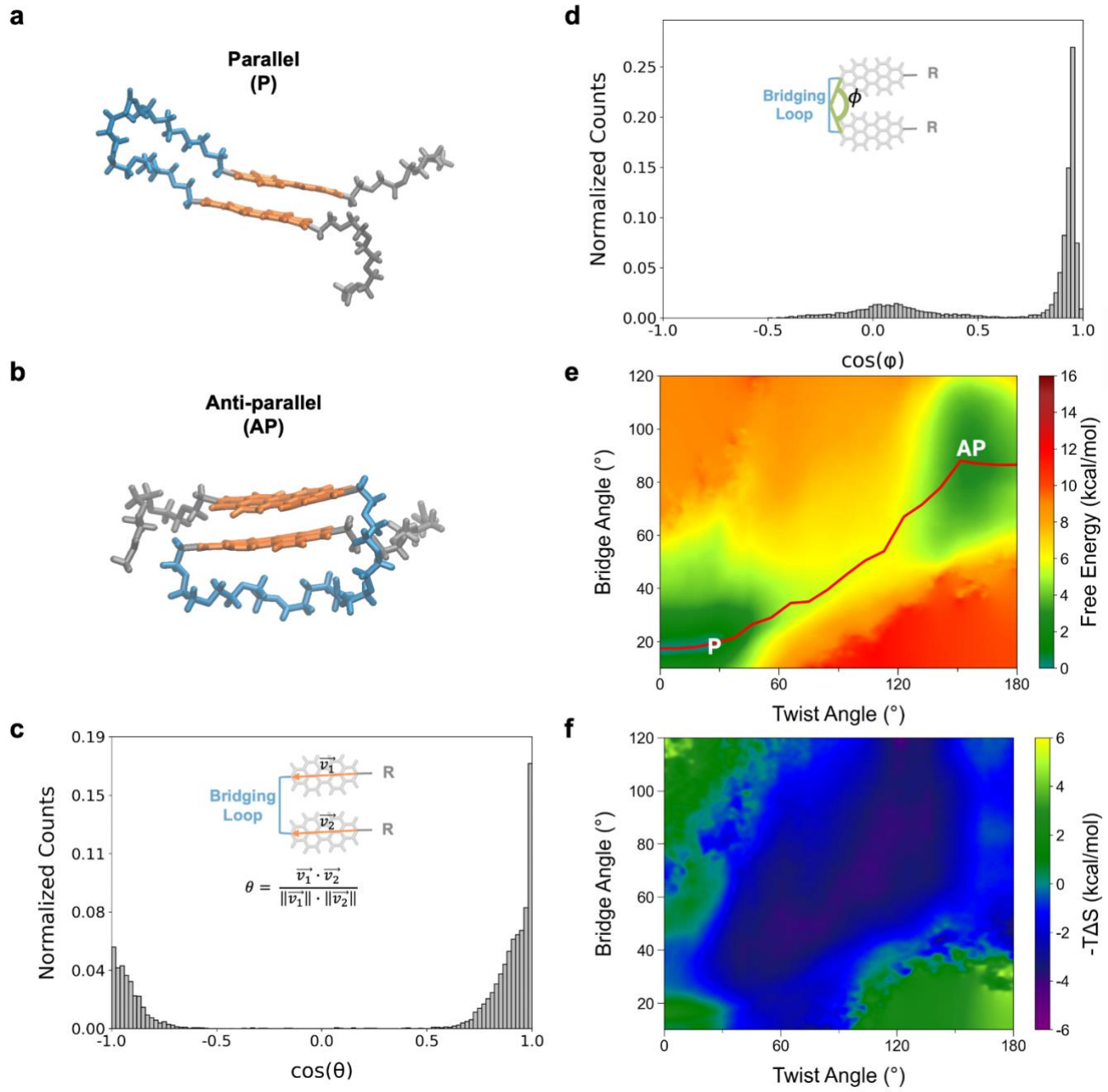

Figure 2. Conformations revealed by MD. (a-b) Simulation snapshots of PDI dimers (orange) in *parallel* (a) and *anti-parallel* (b) orientations, connected by a bridging loop (blue) that adopts distinct spatial arrangements. (c-d) Schematic representation of the twist angle q and the bridge angle ϕ and their distribution along a 1 ms MD production where the system of interest is unrestrained in acetonitrile. (e) Free energy and (f) -TΔS computed at 298 K as a function of the bridge and twist angles. The red line on the free energy surface (e) highlights the minimum energy pathway for the conformational transition between the *parallel* and *anti-parallel* conformers.

The two conformers have a small free-energy difference of about 2.8 kcal·mol^{-1} (Fig. S6c). The *parallel* conformer is slightly more stable, which is consistent with the observation that the *parallel* conformation is prevalent in the unbiased simulations (Fig. 2d). The existence of two stable conformations observed in MD suggest the possibility

of two different unfolding processes associated with the bimodal distribution of rupture forces observed in the AFM pulling experiments (Fig. 1d).

To uncover the unfolding mechanism during AFM pulling experiments, we performed steered molecular dynamics (SMD) simulations, in which a mechanical force is applied at the free end of one tetraethylene glycol methyl ester chain, while the position of the other free end of the molecular system is fixed.

Starting from the *anti-parallel* conformer (Fig. 3d, 3e, and 3f), SMD simulations performed at various pulling velocities revealed a consistent single dimeric rupture pathway. Dissociation proceeds *via* sliding one PDI over the other, during which the pulling force initially increases, followed by a sudden force drop corresponding to the rupture event. The robustness of this mechanism across a range of pulling velocities suggests that the *anti-parallel* form defines a dominant dissociation pathway. Remarkably, SMD simulations starting from the *parallel* conformer (Fig. 3a, 3b, and 3c) reveal an additional intermediate step. When an external force is applied, the PDI dimer undergoes first a transition from the *parallel* to the *anti-parallel* form. This is characterized by a rotation of the PDI units relative to each other, which increases both the twist and the bridge angles. Notably, even though the distance between the PDI planes remains unchanged after the conformational rearrangement, the total molecular extension is increased by 0.7–1.1 nm and appear as a transient force drop (Fig. 3a). After this rearrangement, the mechanical extension resumes to complete the rupture process as observed for the *anti-parallel* conformation.

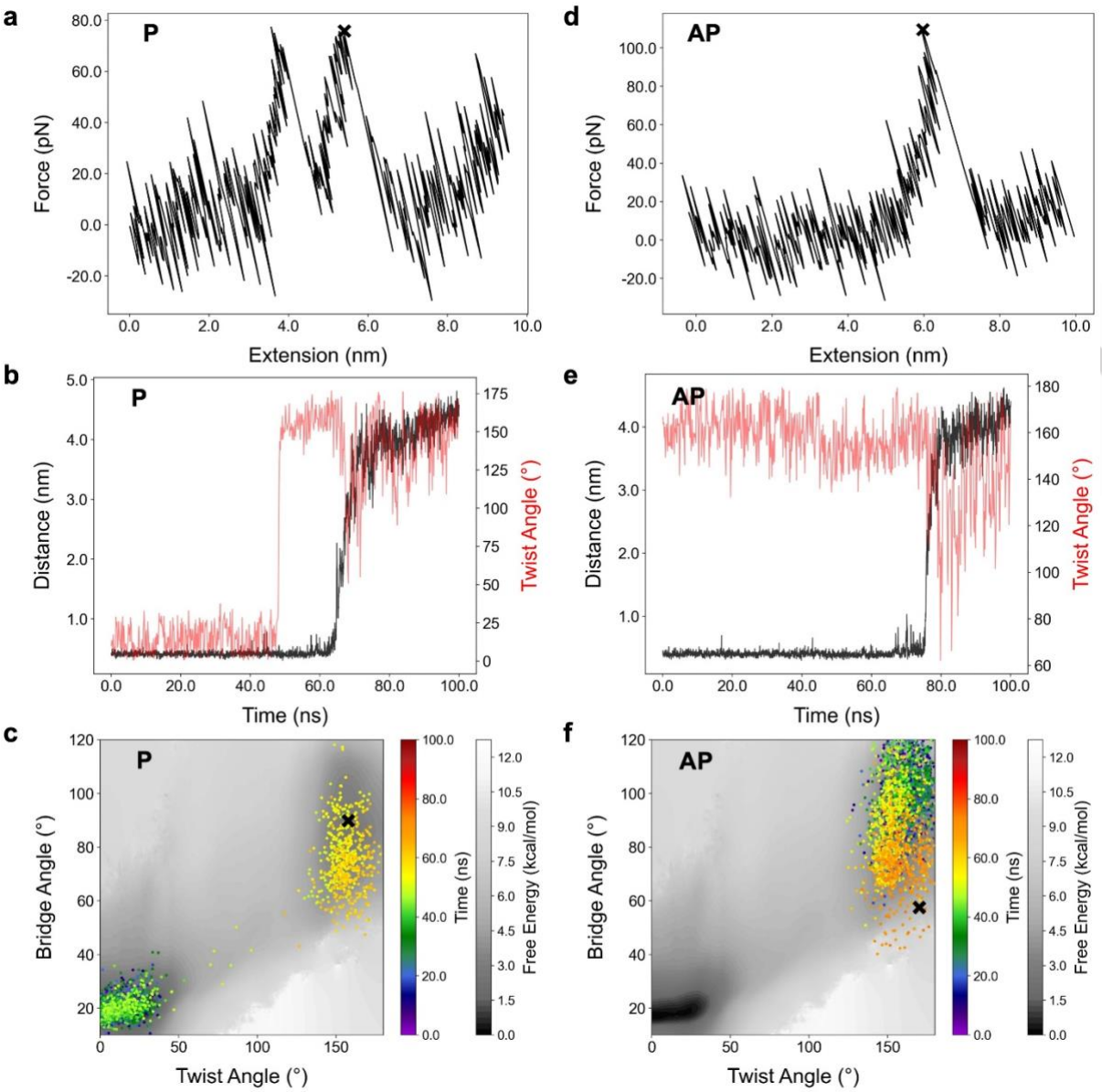

Figure 3. Force and structural changes in PDI dimers during SMD simulations at a pulling velocity of 0.0000010 Å/fs. Profiles are shown for *parallel* (P) and *anti-parallel* (AP) conformations. (a) Force-extension profile, (b) distance (PDI's centre of mass)-time profile, and (c) observed angle values before rupture during an SMD simulation starting from a *parallel* conformation. (d) Force-extension profile, (e) distance (PDI's centre of mass)-time profile, and (f) observed angle values during an SMD simulation starting from an *anti-parallel* conformation. Black crosses indicate the rupture time of the PDI-dimer interaction (64.3 ns for P; 75.3 ns for AP).

During the SMD simulations, we did not observe any direct transition from the *parallel* to the unfolded form: the free energy cost of this process is too high and the dissociation of the PDI dimer always proceeds through the minimum free energy path, namely *via* the a*nti-parallel* conformation acting as an intermediate state. Similarly, the *anti-parallel* conformer rarely exhibited PDI rotation to recover the *parallel* one during the pulling process, suggesting a kinetically stabilised *anti-parallel* conformer, owing to the presence of the bridging loop encircling the dimer (Fig. 2a).

Intermediate unfolding step unveiled by passive force spectroscopy

Based on active SMFS observations, we cannot unambiguously correlate the two populations of rupture forces (F_{peak}, Fig. 1d) to the two unfolding pathways of *parallel/anti-parallel* conformations predicted by SMD simulations. Indeed, the experiments, carried out at a constant pulling velocity, consistently result in the same double-peak pattern, corresponding to the folded-to-unfolded transition followed by the molecule detachment. Unlike in the simulations, no intermediate step is evidenced. The small variation in total molecular extension expected for the *parallel* to *anti-parallel* conformational change (about 1 nm) is within the error of the Δx distribution (5.1 ± 1.9 nm) and is very close to the *z* spatial resolution of our AFM setup, preventing us from discriminating *parallel* and *anti-parallel* populations and observing this conformational change in real time by active SMFS.

To circumvent the spatial resolution limitation encountered in active SMFS experiments and to elucidate the mechanics of the PDI dimers under external force, we further employed passive force spectroscopy at the single-molecule level[10,54]. In this experiment, the macromolecule interfaced between the AFM tip and the substrate is stretched until reaching a certain threshold force. Then, the stretching is halted, and the system extension (*clamping* extension) is maintained for a few seconds. During this *clamping* time, the molecule's response is directly observed before its detachment from the tip. Typically, the force-time (F-t) graph of a conventional polymer chain in a passive force mode only presents a single plateau curve (Fig. S5). This profile was frequently observed during our experiments and corresponds to the polymer chain being maintained exactly at the same force and extension for a short time before detaching from the tip. Remarkably, we also observed singular patterns featuring three or two subsequent plateaus in the F-t curves (examples shown in Fig. 4a and 4d). To permit an effective real-time probing of the folded conformers, one needs to apply a sufficient mechanical load. In fact, we observed multiple plateaus only when the clamping force approached the force required to break a single PDI dimer interaction (previously determined by active SMFS).

Each plateau is characterized by a precise force and extension (*i.e*. the clamping F-E locations, shown as black dots in Fig. 4b and 4e), and a lifetime τ of the conformation (*i.e*. the time spent at the F-E position during the passive mode). Given that each F-E position is held for a sufficient time (longer compared to active SMFS), it is possible to determine potential intermediate steps in the unfolding process with a higher spatial resolution. To attribute the plateaus obtained during passive SMFS to precise folded and unfolded PDI-PDI conformations, we characterized the plateaus' forces and extensions, associated with their lifetimes τ (Table S1).

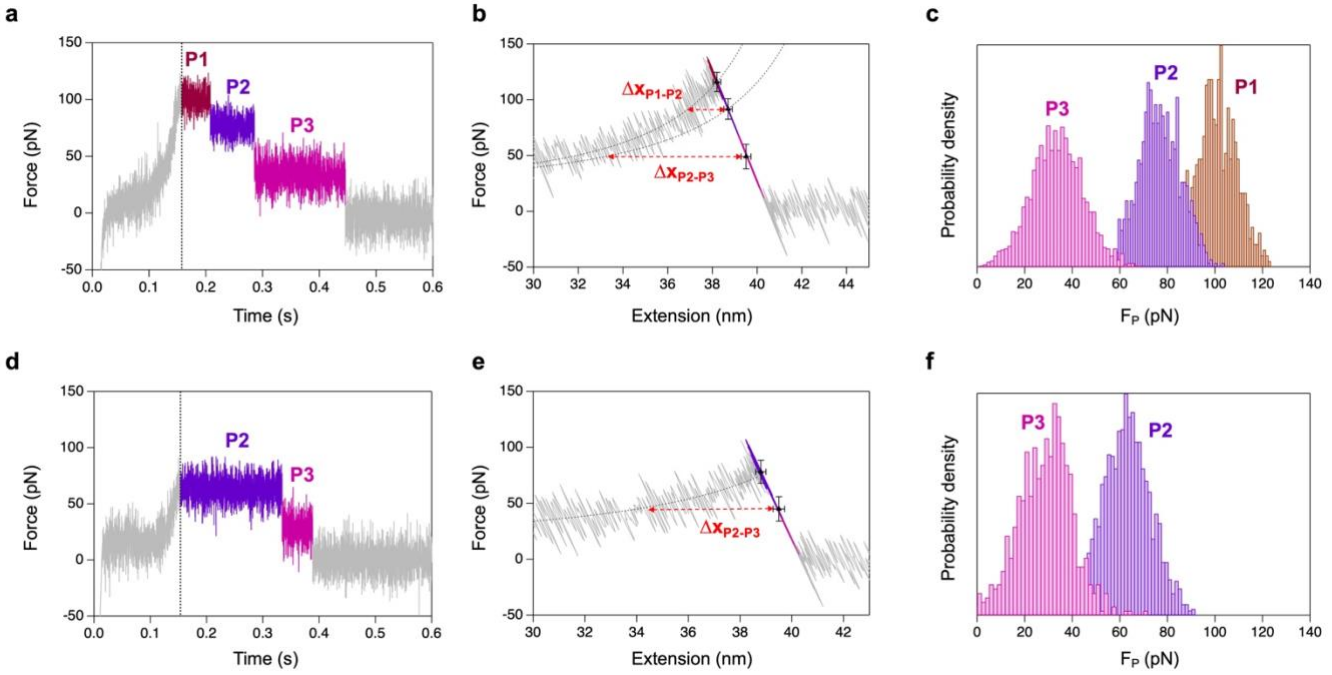

Figure 4. PDI dimers under passive SMFS. The PDI dimers are stretched to the clamping extension, and the force applied by the molecule on the AFM tip is observed in real time. Two characteristic signatures in acetonitrile are presented with corresponding F-t curves (dotted lines mark the start of the *clamping*), F-E curves, and plateau force distributions. Examples of a triple-plateau profile (a) and double-plateau profile (d) represent the unfolding pathways from the *parallel* and *anti-parallel* conformations respectively. The revealed length Δx is measured on F-E curves (b and e): $\Delta x_{P1\text{-}P2}$ = 1.6 ± 0.4 nm and $\Delta x_{P2\text{-}P3}$ = 5.1 ± 2.0 nm, which confirms the attribution of *P1*, *P2,* and *P3* to the *parallel*, *anti-parallel,* and *unfolded* conformations respectively. The distributions of force values (F_p) for *P1* and *P2* (c and f) are also consistent with the force values observed in active SMFS experiments.

In Fig. 4a, the first plateau is characterized by a plateau force of F_{P1} = 107 ± 28 pN, the second one F_{P2} = 72 ± 22 pN and the third one F_{P3} = 41 ± 19 pN (distributions in Fig. 4c). The plateau force values of *P1* and *P2* are close to the values of rupture force determined during active SMFS measurements, which could indicate the observation of the two folded conformations evidenced by simulations (*parallel* and *anti-parallel,* respectively). The third plateau is attributed to the unfolded conformation after the rupture of the PDI dimer interaction. The revealed length Δx, related to the first rupture (*P1* to *P2*) and the second rupture (*P2* to *P3*), was measured on 9 successful clamping experiments. The Δx value is calculated on the F-E curve at identical force (red dotted arrows in Fig. 4b and 4e) to exclude the effect of the polymer extensibility under load. The revealed length from *P2* to *P3* is $\Delta x_{P2\text{-}P3}$ = 5.1 ± 2.0 nm, again confirming the attribution of *P3* to the unfolded conformation (after the rupture of the PDI-PDI interaction revealing the bridging loop), and *P2* to one folded conformation. The value of $\Delta x_{P1\text{-}P2}$ = 1.6 ± 0.4 nm is much smaller and can be attributed to the transition from the *parallel* conformation to the *anti-parallel* conformation. Thus, we attribute P1 and P2 states respectively to the *parallel* and *anti-parallel* conformations.

Hence, during a passive SMFS experiment, when a PDI dimer in a *parallel* conformation is stretched to a clamping force value close to ~120 pN (high force population in active SMFS, Fig. 1d), the dimer can sustain the external force for a period τ_1 before switching to its *anti-parallel* form, revealing a small extension of about 1 nm. Under tension, this transition is irreversible and leads to the observation of the *anti-parallel* conformation (with a lifetime

τ_2) that will eventually unfold with a revealed extension of about 5 nm, corresponding precisely to the length of the bridging loop (Fig. 5a).

Contrarily, when a PDI dimer is already in an *anti-parallel* conformation, only 2 plateaus (*e.g*. *P2* and *P3* in Fig. 4d) can be observed before the detachment of the molecule from the tip, respectively corresponding to the *anti-parallel* and unfolded conformations.

Overall, we can conclude that the unfolding mechanisms revealed by passive SMFS experiments closely match those predicted by SMD simulations (Fig. 5a). Moreover, we can emphasize the fact that the force measured in SMFS consists of a direct probe of the potential energy surface around the different stable states of the PDI dimer system. Indeed, the free enthalpy profile as a function of the twist angle θ (see Fig. S6c and SI for details) presents a steeper slope (details in SI) associated with the *parallel* minimum as compared to the *anti-parallel* one, consistently with the larger forces (i) observed in the *parallel* conformation in the passive mode SMFS and (ii) to unfold the system from this state in active SMFS, compared to the *anti-parallel* conformation.

Unfolding *parallel* conformers requires higher force and work

Given that SMFS experiments are performed outside the thermodynamic equilibrium of the noncovalent interaction, we cannot directly extract the PDI-PDI rupture energy from force measurements; a non-negligible portion of the work required to break the interaction is dissipated during stretching. Instead, we compare the work required to mechanically trigger the conformational changes during both active and passive SMFS experiments. This work was quantified as the area below the F-E curve during the transition, *i.e*. the transition from one conformation to the other, eliminating the contribution originating from the extension of the macromolecular linkers during the transition (Fig. S6a).

In passive force spectroscopy, the work associated with the conformational change between two F-E clamping positions (or two plateaus) is $W_{P1\text{-}P2}$ = 1.5 ± 1.4 kcal·mol^{-1} and $W_{P2\text{-}P3}$ = 1.9 ± 1.0 kcal·mol^{-1}. The unfolding work of the *anti-parallel* conformer is thus obtained as $W_{anti-parallel}^{passive}$ = $W_{P2\text{-}P3}$ = 1.9 ± 1.0 kcal·mol^{-1}. Given the stepwise unfolding pathway observed for the *parallel* conformer by SMD and confirmed by passive SMFS, its unfolding work is therefore higher and can be estimated to $W_{parallel}^{passive} \approx W_{P1\text{-}P2} + W_{P2\text{-}P3}$ = 3.4 ± 2.4 kcal·mol^{-1}.

In active force spectroscopy (pulling velocity of 10^2 nm·s^{-1}), we also quantified the unfolding work associated with the first force peak in double-peak patterns. The distribution of work (Fig. S6b) presents two populations at 2.8 ± 1.3 kcal·mol^{-1} (67%) and 7.0 ± 3.2 kcal·mol^{-1} (33 %). These work populations correlate with the peak force populations observed in active force spectroscopy and can thus be attributed to the unfolding works $W_{anti-parallel}^{active}$ and $W_{parallel}^{active}$ respectively. The unfolding work values obtained from the SMD simulations (pulling velocity of 10^8 nm·s^{-1}) are substantially higher: $W_{anti-parallel}^{SMD}$ = 15.8 ± 3.3 kcal·mol^{-1} and $W_{parallel}^{SMD}$ = 20.7 ± 2.6 kcal·mol^{-1}. The increase of the unfolding work (or rupture force) with the loading rate is well-known, especially when comparing force spectroscopy measurements and simulations that take place at different pulling velocities (several orders of

magnitude higher for simulations).[60] In all cases, we observe a higher work required to unfold the *parallel* conformer compared to the *anti-parallel* one, even in the case of active SMFS. As explained before, this increased work is consistent with a stepwise unfolding pathway for the *parallel* conformer— first a rotation of PDI units and then a sliding of one unit over the other one— and supports its higher mechanical resistance to external stress.

Unfolding kinetics of a single PDI dimer

When considering passive SMFS, we notice that one PDI dimer under an external force is able, after a sufficiently long time τ_F and under a force F, to overcome the energetic barrier and reach another conformation. Therefore, following the attribution of each plateau pattern in passive SMFS to one conformation of the PDI dimer, we have investigated the lifetime variation of both folded states. Fig. 5b reveals the correlation between the lifetimes τ_1 and τ_2 (respectively *parallel* and *anti-parallel* conformations) as a function of the plateau forces F_{P1} and F_{P2} for 9 successful clamping experiments. The evolutions of the observed lifetime of the conformations under load illustrate well the Arrhenius law relating the kinetics of a physical bond rupture to overcome an activation barrier. In our case, we observed a strong effect of the force on the lifetime of each conformation. Both evolutions were analysed and fitted with the Bell-Evans equation:

$$\tau(F) = \tau(0)\, e^{\frac{-Fx_\beta}{k_B T}}$$

where F is the clamping force, τ the lifetime of each conformation, $\tau(0)$ the lifetime at zero force, x_b the distance to the energetic barrier, k_β the Boltzmann constant, and T the temperature.

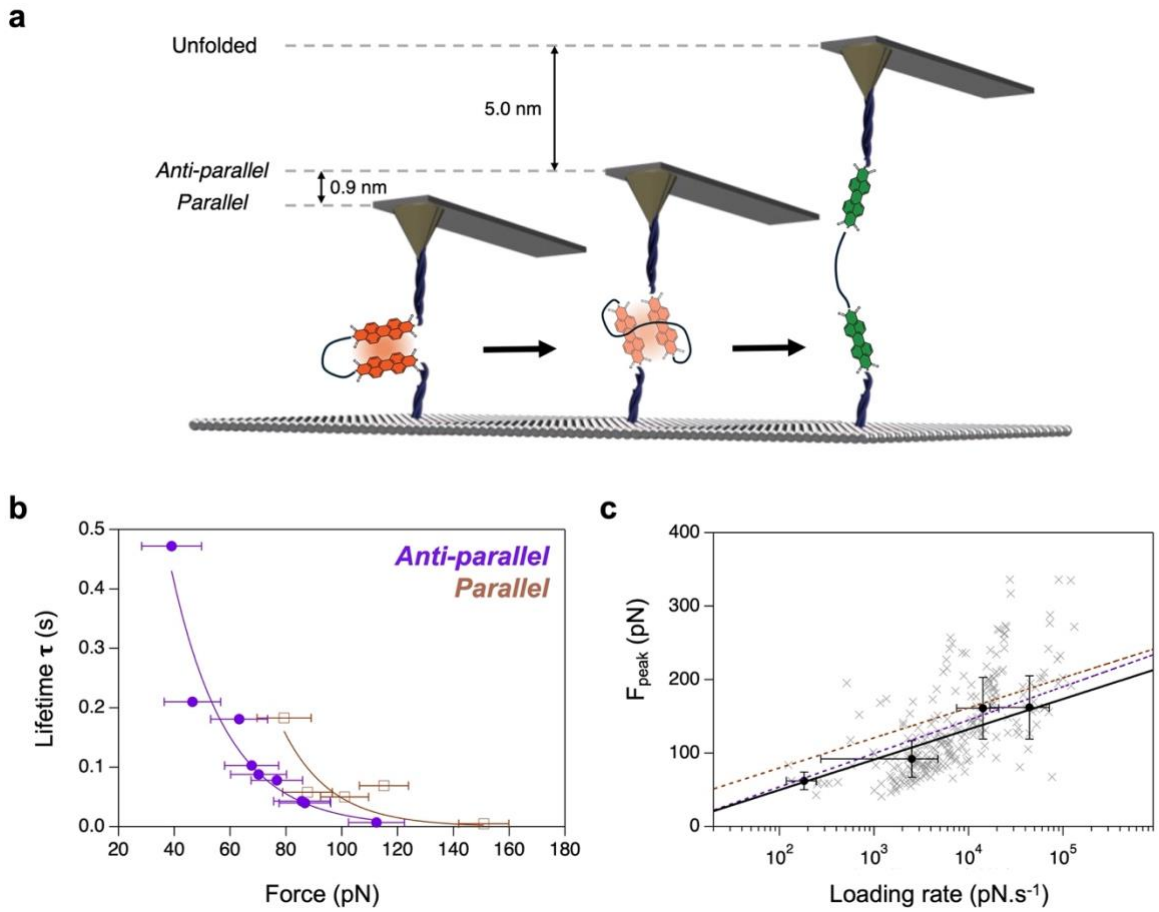

Figure 5. Unfolding mechanisms and kinetics of *parallel* and *anti-parallel* conformers. (a) Scheme of the mechanical unfolding mechanisms from the *parallel* (*left*), *via* the *anti-parallel* (*central*), to the unfolded conformation (*right*). The simulated extension increases for both steps are respectively of 0.9 nm and 5.1 nm, in agreement with the values observed in passive SMFS. (b) The plateau times observed in passive SMFS in relation to the plateau force correspond to a Bell-Evans law, evidencing different *parallel* (brown squares) and *anti-parallel* (purple dots) conformational stabilities. Bell-Evans fits revealed the positions of the energetic barriers $x_\beta \approx 0.2$ nm, in agreement with values obtained from MD (details in SI). (c) Dynamic force spectroscopy experiments show a similar Bell-Evans evolution of the rupture force (active SMFS) with the loading rate (N = 260). Gray crosses correspond to individual force peaks (in *double peak* profiles) and black dots are central values of F_{peak} and r. The Bell-Evans fitting curves obtained from passive SMFS (brown for *parallel* and purple for *anti-parallel* conformations) are added as dotted lines for comparison.

Considering the position of the energetic barrier, we found $x_{\beta,\mathrm{anti-parallel}}^{passive}$ = 0.21 ± 0.03 nm for the *anti-parallel* conformation and $x_{\beta,\mathrm{parallel}}^{passive}$ = 0.24 ± 0.12 nm for the *parallel* conformation (Bell-Evans fits in purple and brown respectively in Fig. 5b and c). The almost identical x_β values originate from the similarity of the PDI-PDI interaction in both conformations. The PDI-PDI interacting distance, typically of 3.5 Å for both folded states, requires an increase of about 2 Å (x_β value) to trigger the π-interaction rupture, leading to the separation (or misalignment) of the dimer.

The Bell-Evans description of a bond lifetime can also be supported by the dynamic evolution of the rupture force (F_{peak}) of one interaction in relation to the experimental loading rate (r) applied in active SMFS experiments.[49,61]

Fig. 5c shows the dynamic force spectrum (DFS) of the PDI dimers stretched at various loading rates ranging from 10^2 to 10^5 pN·s^{-1} (details in SI). As explained before, populations from *parallel* and *anti-parallel* conformations cannot be unambiguously distinguished in the DFS evolution (limited resolution in active SMFS), and the polymer linkers here lead to a significant broadening of the force distributions.[61] Nevertheless, the distribution of F_{peak} *vs r* was adjusted by a Bell-Evans[60] fit, which returned x_{β}^{active} = 0.23 ± 0.07 nm, very close to the values obtained by the lifetime analysis in passive SMFS. The fidelity of both analyses is illustrated by the reconstructions of the Bell-Evans evolutions obtained from passive force measurements (purple and brown lines) in the DFS graph (Fig. 5c), showing very similar behaviours. Similarly, the SMD simulations at higher pulling velocities also returned very similar values for the energetic barrier position: $x_{\beta,\mathrm{parallel}}^{SMD}$ = 0.24 ± 0.04 nm and $x_{\beta,\mathrm{anti-parallel}}^{SMD}$= 0.19 ± 0.03 nm (Fig. S11).

When considering instead the unbinding kinetic rate (k_{off}, calculated as the inverse of $\tau(0)$), we noted a large difference in the values extracted from the Bell-Evans analyses in AFM data and from the SMD simulations (Table S2). This difference originates from the very different loading rates employed and the use of a flexible polymer linker in the AFM experiments that can act as an additional soft link and bias the kinetic parameters identified for the PDI dimers. Yet, the k_{off} values obtained experimentally support a lower unfolding rate for the *parallel* conformer that is explained by the different spatial arrangement of the bridging loop around the folded states associated with a small but existing free energy difference between *parallel* and *anti-parallel* conformers. Thus, in addition to routine dynamic force spectroscopy approaches, the study of the conformational lifetimes performed here by passive SMFS adds precise information about the unfolding energetic pathways and the force-induced mechanics of the PDI-PDI interaction rupture.

Conclusion

Mechano-responsive molecular motifs, such as perylene diimide derivatives, have already been used in materials for their fast response and reversible behaviour under external stress. A detailed description of the molecular conformational changes that occur under mechanical stress is difficult to obtain using ensemble techniques, despite the high importance of these processes for the rational design of chemically precise architectures. Advanced single-molecule techniques of such mechano-responsive motifs are now crucial. Here, we have employed advanced AFM-based single-molecule force spectroscopy experiments and molecular dynamic simulations to precisely describe the folded states of PDI dimers and to uncover the force-induced unfolding pathways.

We have modified a looped PDI dimer with flexible polymers for AFM interfacing, with a strong anchoring strategy for stable passive force spectroscopy experiments. Active SMFS in acetonitrile revealed the force signature of individual dimers and suggested two folded geometries associated with distinct unfolding forces. Molecular dynamics on the PDI dimer revealed these folding conformations, which comprise oppositely oriented PDIs, namely the *parallel* and *anti-parallel* conformers. The simulated optimized geometries revealed the effect of the bridging loop, which surrounds the PDI units in an *anti-parallel* conformation and therefore affects the unfolding kinetics.

The unfolding mechanisms were described by steered molecular dynamics starting from both folded conformations. While the *anti-parallel* conformer unfolds in a single step as the mechanical force is aligned with the PDIs, the *parallel* dimer undergoes a local reorganization of the PDI units toward the *anti-parallel* conformer before force-induced unfolding. This two-step unfolding mechanism has been described energetically, evidencing a favoured pathway '*parallel* to *anti-parallel* to *unfolded*' compared to the straightforward unfolding of the *parallel* conformer, which was not observed. Interestingly, this unfolding pathway has also been observed in real time during passive force spectroscopy experiments. Despite the very small conformational difference between the *parallel* and *anti-parallel* forms, we were able to probe and discriminate them, and to measure their respective lifetimes under mechanical stress. We showed that the difference in the unfolding mechanisms is associated with a difference in mechanical work required for the unfolding (higher for the *parallel* conformer), measured by SMFS and simulations. This difference in mechanical stability originates from the spatial arrangement of the loop bridging both PDI units, impacting the *parallel* or *anti-parallel* orientation of the PDIs and thus their unfolding mechanisms. It is worth emphasizing the high similarity between the MD simulations and the thermodynamic analysis of passive force spectroscopy experiments. This coupled method uncovered two distinct folded conformations that were hidden by standard ensemble techniques and provided a high-resolution, detailed description of the rupture of noncovalent interactions in perylene diimide dimers. Furthermore, the energetic description of both unfolding pathways and the illustration of the kinetic laws governing noncovalent interactions highlight the effectiveness and accuracy of our combined single-molecule approach. This methodology offers the requisite precision to distinguish conformers that were not accessible with existing approaches, but also provides access to unfolding mechanisms and direct measurements of individual π-interaction lifetimes under force. We emphasize the importance of this approach for the rigorous mechanochemical description of noncovalent molecular systems to be integrated in responsive materials.

Supporting Information

The authors have cited additional references within the Supporting Information.[62–73]

Acknowledgements

This work was supported by the European Research Council (ERC Advanced Grant 101054338, A.-S.D), the Excellence of Science (EOS 40007519, A.-S.D.) program from the FWO and Fonds de la Recherche Scientifique-FNRS, and FRS-FNRS MIS Grant n° F.4555.26 (D.S.). This research used resources from the "Plateforme Technologique de Calcul Intensif (PTCI)" (http://ww.ptci.unamur.be) located at the University of Namur, Belgium, which is supported by the FNRS-FRFC, the Walloon Region, and the University of Namur (conventions no.2.5020.11, GEQ U.G006. 15, 1610468, RW/GEQ2016 et U.G011.22). The PTCI is a member of the "Consortium des Equipments de Calcul Intensif (CECI)" (http://ww.ceci-hpc.be). The present research also benefited from the computational resources made available on Lucia, the Tier-1 supercomputer of the Walloon Region, infrastructure funded by the Walloon Region under the grant agreement no 1910247. D.B. acknowledges a grant from the ''Fonds pour la formation à la Recherche dans l'Industrie et dans l'Agriculture'' (FRIA) of the FRS-FNRS. The authors also

gratefully acknowledge financial support through National Center of Competence in Research Bio-Inspired Materials, a research instrument of the Swiss National Science Foundation (SNSF, Grant No. 51NF40-18288134), the Swiss National Science Foundation (PR00P2_208616, J.C.) and the Adolphe Merkle Foundation. The authors thank Prof. Stephen Schrettl (Technical University of Munich) for early discussions on this research project.

Keywords: single-molecule force spectroscopy • conformational dynamics • noncovalent interactions • AFM • mechanochemical pathways

References

[1] M. M. Caruso, D. A. Davis, Q. Shen, S. A. Odom, N. R. Sottos, S. R. White, J. S. Moore, "Mechanically-induced chemical changes in polymeric materials" *Chem. Rev.* **2009**, *109*, 5755–5798.

[2] J. Chung, A. M. Kushner, A. C. Weisman, Z. Guan, "Direct correlation of single-molecule properties with bulk mechanical performance for the biomimetic design of polymers" *Nat. Mater.* **2014**, *13*, 1055–1062.

[3] A. M. Kushner, V. Gabuchian, E. G. Johnson, Z. Guan, "Biomimetic design of reversibly unfolding cross-linker to enhance mechanical properties of 3D network polymers" *J. Am. Chem. Soc.* **2007**, *129*, 14110–14111.

[4] Y. Ma, C. Weder, F. E. Du Prez, J. A. Berrocal, "From β-Dicarbonyl Chemistry to Dynamic Polymers" *Chem. Rev.* **2025**, *125*, 9296–9331.

[5] A. L. B. Ramirez, Z. S. Kean, J. A. Orlicki, M. Champhekar, S. M. Elsakr, W. E. Krause, S. L. Craig, "Mechanochemical strengthening of a synthetic polymer in response to typically destructive shear forces" *Nat. Chem.* **2013**, *5*, 757–761.

[6] A. Herzog-Arbeitman, I. Kevlishvili, D. Sen, J. Lian, J. Chakraverty, P. Mueller, S. Wang, B. D. Olsen, H. J. Kulik, S. L. Craig, J. A. Johnson, "Tetrafunctional cyclobutanes tune toughness via network strand continuity" *Nat. Chem.* **2026**, *18*, 309–316.

[7] D. J. Lundberg, C. M. Brown, E. O. Bobylev, N. J. Oldenhuis, Y. S. Alfaraj, J. Zhao, I. Kevlishvili, H. J. Kulik, J. A. Johnson, "Nested non-covalent interactions expand the functions of supramolecular polymer networks" *Nat. Commun.* **2024**, *15*, 3951.

[8] J. Wang, T. B. Kouznetsova, S. L. Craig, "Single-Molecule Observation of a Mechanically Activated *Cis* -to- *Trans* Cyclopropane Isomerization" *J. Am. Chem. Soc.* **2016**, *138*, 10410–10412.

[9] H. Zhang, X. Li, Y. Lin, F. Gao, Z. Tang, P. Su, W. Zhang, Y. Xu, W. Weng, R. Boulatov, "Multi-modal mechanophores based on cinnamate dimers" *Nat. Commun.* **2017**, *8*, 1147.

[10] Y. Zhang, Z. Wang, T. B. Kouznetsova, Y. Sha, E. Xu, L. Shannahan, M. Fermen-Coker, Y. Lin, C. Tang, S. L. Craig, "Distal conformational locks on ferrocene mechanophores guide reaction pathways for increased mechanochemical reactivity" *Nat. Chem.* **2021**, *13*, 56–62.

[11] B. H. Bowser, S. L. Craig, "Empowering mechanochemistry with multi-mechanophore polymer architectures" *Polym. Chem.* **2018**, *9*, 3583–3593.

[12] M. K. Beyer, H. Clausen-Schaumann, "Mechanochemistry: The Mechanical Activation of Covalent Bonds" *Chem. Rev.* **2005**, *105*, 2921–2948.

[13] Y. Li, B. Xue, J. Yang, J. Jiang, J. Liu, Y. Zhou, J. Zhang, M. Wu, Y. Yuan, Z. Zhu, Z. J. Wang, Y. Chen, Y. Harabuchi, T. Nakajima, W. Wang, S. Maeda, J. P. Gong, Y. Cao, "Azobenzene as a photoswitchable mechanophore" *Nat. Chem.* **2024**, *16*, 446–455.

[14] J. Wang, T. B. Kouznetsova, Z. Niu, M. T. Ong, H. M. Klukovich, A. L. Rheingold, T. J. Martinez, S. L. Craig, "Inducing and quantifying forbidden reactivity with single-molecule polymer mechanochemistry" *Nat. Chem.* **2015**, *7*, 323–327.

[15] B. Lee, Z. Niu, S. L. Craig, "The Mechanical Strength of a Mechanical Bond: Sonochemical Polymer Mechanochemistry of Poly(catenane) Copolymers" *Angewandte Chemie* **2016**, *128*, 13280–13283.

[16] C. J. Bruns, J. Fraser Stoddart, *The Nature of the Mechanical Bond: From Molecules to Machines*, **2017**.

[17] M. Zhang, G. De Bo, "Impact of a Mechanical Bond on the Activation of a Mechanophore" *J. Am. Chem. Soc.* **2018**, *140*, 12724–12727.

[18] T. Muramatsu, Y. Okado, H. Traeger, S. Schrettl, N. Tamaoki, C. Weder, Y. Sagara, "Rotaxane-Based Dual Function Mechanophores Exhibiting Reversible and Irreversible Responses" *J. Am. Chem. Soc.* **2021**, *143*, 9884–9892.

[19] H. Xing, Z. Li, Z. L. Wu, F. Huang, "Catenane Crosslinked Mechanically Adaptive Polymer Gel" *Macromol. Rapid Commun.* **2018**, *39*, DOI 10.1002/marc.201700361.

[20] H. Li, H. Zhang, A. D. Lammer, M. Wang, X. Li, V. M. Lynch, J. L. Sessler, "Quantitative self-assembly of a purely organic three-dimensional catenane in water" *Nat. Chem.* **2015**, *7*, 1003–1008.

[21] G. Liu, P. M. Rauscher, B. W. Rawe, M. M. Tranquilli, S. J. Rowan, "Polycatenanes: synthesis, characterization, and physical understanding" *Chem. Soc. Rev.* **2022**, *51*, 4928–4948.

[22] L. F. Hart, J. E. Hertzog, P. M. Rauscher, B. W. Rawe, M. M. Tranquilli, S. J. Rowan, "Material properties and applications of mechanically interlocked polymers" *Nat. Rev. Mater.* **2021**, *6*, 508–530.

[23] H. Traeger, Y. Sagara, D. J. Kiebala, S. Schrettl, C. Weder, "Folded Perylene Diimide Loops as Mechanoresponsive Motifs" *Angew. Chem. Int. Ed.* **2021**, *60*, 16191–16199.
[24] A. Haque, K. M. Alenezi, M. S. Khan, W.-Y. Wong, P. R. Raithby, "Non-covalent interactions (NCIs) in π-conjugated functional materials: advances and perspectives" *Chem. Soc. Rev.* **2023**, *52*, 454–472.
[25] K. Carter-Fenk, J. M. Herbert, "Reinterpreting π-stacking" *Physical Chemistry Chemical Physics* **2020**, *22*, 24870–24886.
[26] P. Liu, S. Jimaja, S. Immel, C. Thomas, M. Mayer, C. Weder, N. Bruns, "Mechanically triggered on-demand degradation of polymers synthesized by radical polymerizations" *Nat. Chem.* **2024**, *16*, 1184–1192.
[27] H. Traeger, Y. Sagara, J. A. Berrocal, S. Schrettl, C. Weder, "Strain-correlated mechanochromism in different polyurethanes featuring a supramolecular mechanophore" *Polym. Chem.* **2022**, *13*, 2860–2869.
[28] C. Micheletti, L. Soldati, C. Weder, A. Pucci, J. M. Clough, "Mechanochromic Polyolefin Elastomers" *ACS Appl. Polym. Mater.* **2024**, *6*, 6572–6580.
[29] Y. Sagara, H. Traeger, J. Li, Y. Okado, S. Schrettl, N. Tamaoki, C. Weder, "Mechanically Responsive Luminescent Polymers Based on Supramolecular Cyclophane Mechanophores" *J. Am. Chem. Soc.* **2021**, *143*, 5519–5525.
[30] A. Germann, J. Meisner, "Force-induced transition state rupture enables mechanistic control in aziridine mechanochemistry" *Chem. Sci.* **2025**, *16*, 21454–21463.
[31] Y. Zhang, C. Liu, W. Shi, Z. Wang, L. Dai, X. Zhang, "Direct measurements of the interaction between pyrene and graphite in aqueous media by single molecule force spectroscopy: Understanding the π-π interactions" *Langmuir* **2007**, *23*, 7911–7915.
[32] C. J. Bustamante, Y. R. Chemla, S. Liu, M. D. Wang, "Optical tweezers in single-molecule biophysics" *Nature Reviews Methods Primers* **2021**, *1*, 25.
[33] C. Bustamante, S. Yan, "The development of single molecule force spectroscopy: from polymer biophysics to molecular machines" *Q. Rev. Biophys.* **2022**, *55*, e9.
[34] K. Bian, C. Gerber, A. J. Heinrich, D. J. Müller, S. Scheuring, Y. Jiang, "Scanning probe microscopy" *Nature Reviews Methods Primers* **2021**, *1*, 36.
[35] Y. Bao, Z. Luo, S. Cui, "Environment-dependent single-chain mechanics of synthetic polymers and biomacromolecules by atomic force microscopy-based single-molecule force spectroscopy and the implications for advanced polymer materials" *Chem. Soc. Rev.* **2020**, *49*, 2799–2827.
[36] Z.-H. Zhang, H.-N. Feng, G. Chi, D. A. Leigh, L. Zhang, "Single-Molecule Studies on Artificial Small-Molecule Machines" *CCS Chemistry* **2023**, *5*, 2448–2465.
[37] M. J. Jacobs, K. Blank, "Joining forces: integrating the mechanical and optical single molecule toolkits" *Chem. Sci.* **2014**, *5*, 1680–1697.
[38] A. Narayan, M. T. Woodside, **2025**, Elsevier Ltd preprint, DOI: 10.1016/j.sbi.2025.103110.
[39] S. Garcia-Manyes, A. E. M. Beedle, "Steering chemical reactions with force" *Nat. Rev. Chem.* **2017**, *1*, 0083.
[40] M. Grandbois, M. Beyer, M. Rief, H. Clausen-Schaumann, H. E. Gaub, "How strong is a covalent bond" *Science (1979).* **1999**, *283*, 1727–1730.
[41] J. Wang, T. B. Kouznetsova, Z. Niu, M. T. Ong, H. M. Klukovich, A. L. Rheingold, T. J. Martinez, S. L. Craig, "Inducing and quantifying forbidden reactivity with single-molecule polymer mechanochemistry" *Nat. Chem.* **2015**, *7*, 323–327.
[42] Y. Li, J. Wen, M. Qin, Y. Cao, H. Ma, W. Wang, "Single-Molecule Mechanics of Catechol-Iron Coordination Bonds" *ACS Biomater. Sci. Eng.* **2017**, *3*, 979–989.
[43] M. Muddassir, "Blue light-induced low mechanical stability of ruthenium-based coordination bonds: An AFM-based single-molecule force spectroscopy study" *RSC Adv.* **2020**, *10*, 40543–40551.
[44] X. Li, Y. Gisbert, M. Ledent, D. Sluysmans, G. Rapenne, C. Kammerer, A.-S. Duwez, "Probing the free rotary oscillations around a single ruthenium atom in an organometallic complex" *Chem* **2026**, *12*, 102691.
[45] M. Calvaresi, A. S. Duwez, D. A. Leigh, D. Sluysmans, Y. Song, F. Zerbetto, L. Zhang, "Mechanical tightening of a synthetic molecular knot" *Chem* **2023**, *9*, 65–75.
[46] D. Sluysmans, S. Hubert, C. J. Bruns, Z. Zhu, J. F. Stoddart, A. S. Duwez, "Synthetic oligorotaxanes exert high forces when folding under mechanical load" *Nat. Nanotechnol.* **2018**, *13*, 209–213.
[47] D. Sluysmans, P. Lussis, C. A. Fustin, A. Bertocco, D. A. Leigh, A. S. Duwez, "Real-Time Fluctuations in Single-Molecule Rotaxane Experiments Reveal an Intermediate Weak Binding State during Shuttling" *J. Am. Chem. Soc.* **2021**, *143*, 2348–2352.
[48] F. Devaux, X. Li, D. Sluysmans, V. Maurizot, E. Bakalis, F. Zerbetto, I. Huc, A. S. Duwez, "Single-molecule mechanics of synthetic aromatic amide helices: Ultrafast and robust non-dissipative winding" *Chem* **2021**, *7*, 1333–1346.
[49] D. Sluysmans, F. Devaux, C. J. Bruns, J. Fraser Stoddart, A. S. Duwez, "Dynamic force spectroscopy of synthetic oligorotaxane foldamers" *Proc. Natl. Acad. Sci. U. S. A.* **2018**, *115*, 9362–9366.
[50] A. Van Quaethem, P. Lussis, D. A. Leigh, A. S. Duwez, C. A. Fustin, "Probing the mobility of catenane rings in single molecules" *Chem. Sci.* **2014**, *5*, 1449–1452.
[51] P. Lussis, T. Svaldo-Lanero, A. Bertocco, C. A. Fustin, D. A. Leigh, A. S. Duwez, "A single synthetic small molecule that generates force against a load" *Nat. Nanotechnol.* **2011**, *6*, 553–557.
[52] M. Janke, Y. Rudzevich, O. Molokanova, T. Metzroth, I. Mey, G. Diezemann, P. E. Marszalek, J. Gauss, V. Böhmer, A. Janshoff, "Mechanically interlocked calix[4]arene dimers display reversible bond breakage under force" *Nat. Nanotechnol.* **2009**, *4*, 225–229.
[53] D. Sluysmans, L. Zhang, X. Li, A. Garci, J. F. Stoddart, A. S. Duwez, "Viologen Tweezers to Probe the Force of Individual Donor-Acceptor π-Interactions" *J. Am. Chem. Soc.* **2020**, *142*, 21153–21159.
[54] M. Ledent, Y. Gisbert, D. Sluysmans, R. Astumian, B. Feringa, A.-S. Duwez **2025**, DOI: 10.21203/rs.3.rs-6988620/v1.
[55] T. Naranjo, K. M. Lemishko, S. de Lorenzo, Á. Somoza, F. Ritort, E. M. Pérez, B. Ibarra, "Dynamics of individual molecular shuttles under mechanical force" *Nat. Commun.* **2018**, *9*, 4512.

[56] P. J. Flory, *Statistical Mechanics of Chain Molecules*, Hanser Publishers, **1988**.
[57] B. Schramm, M. Gray, J. M. Herbert, "Substituent and Heteroatom Effects on π–π Interactions: Evidence That Parallel-Displaced π-Stacking is Not Driven by Quadrupolar Electrostatics" *J. Am. Chem. Soc.* **2025**, *147*, 3243–3260.
[58] A. Oleson, T. Zhu, I. S. Dunn, D. Bialas, Y. Bai, W. Zhang, M. Dai, D. R. Reichman, R. Tempelaar, L. Huang, F. C. Spano, "Perylene Diimide-Based Hj- and hJ-Aggregates: The Prospect of Exciton Band Shape Engineering in Organic Materials" *The Journal of Physical Chemistry C* **2019**, *123*, 20567–20578.
[59] B. Mahlmeister, T. Schembri, V. Stepanenko, K. Shoyama, M. Stolte, F. Würthner, "Enantiopure J-Aggregate of Quaterrylene Bisimides for Strong Chiroptical NIR-Response" *J. Am. Chem. Soc.* **2023**, *145*, 13302–13311.
[60] E. Evans, K. Ritchie, "Dynamic strength of molecular adhesion bonds" *Biophys. J.* **1997**, *72*, 1541–1555.
[61] C. Friedsam, A. K. Wehle, F. K hner, H. E. Gaub, "Dynamic single-molecule force spectroscopy: bond rupture analysis with variable spacer length" *Journal of Physics: Condensed Matter* **2003**, *15*, S1709–S1723.
[62] J. Chen, A. W. Ziegler, B. Zhao, W. Wan, A. D. Q. Li, "Chemomechanical-force-induced folding-unfolding directly controls distinct fluorescence dual-color switching" *Chemical Communications* **2017**, *53*, 4993–4996.
[63] Q. Zhang, A. Anastasaki, G.-Z. Li, A. J. Haddleton, P. Wilson, D. M. Haddleton, "Multiblock sequence-controlled glycopolymers via Cu(0)-LRP following efficient thiol–halogen, thiol–epoxy and CuAAC reactions" *Polym. Chem.* **2014**, *5*, 3876–3883.
[64] J. E. Sader, R. Borgani, C. T. Gibson, D. B. Haviland, M. J. Higgins, J. I. Kilpatrick, J. Lu, P. Mulvaney, C. J. Shearer, A. D. Slattery, P. A. Thorén, J. Tran, H. Zhang, H. Zhang, T. Zheng, "A virtual instrument to standardise the calibration of atomic force microscope cantilevers" *Review of Scientific Instruments* **2016**, *87*, DOI 10.1063/1.4962866.
[65] J. C. Phillips, D. J. Hardy, J. D. C. Maia, J. E. Stone, J. V. Ribeiro, R. C. Bernardi, R. Buch, G. Fiorin, J. Hénin, W. Jiang, R. McGreevy, M. C. R. Melo, B. K. Radak, R. D. Skeel, A. Singharoy, Y. Wang, B. Roux, A. Aksimentiev, Z. Luthey-Schulten, L. V. Kalé, K. Schulten, C. Chipot, E. Tajkhorshid, "Scalable molecular dynamics on CPU and GPU architectures with NAMD" *Journal of Chemical Physics* **2020**, *153*, DOI 10.1063/5.0014475.
[66] C. B. Markegard, A. Mazaheripour, J. M. Jocson, A. M. Burke, M. N. Dickson, A. A. Gorodetsky, H. D. Nguyen, "Molecular Dynamics Simulations of Perylenediimide DNA Base Surrogates" *Journal of Physical Chemistry B* **2015**, *119*, 11459–11465.
[67] Frisch, M. J., Trucks, G. W., Schlegel, H. B., Scuseria, G. E., Robb, M. A., Cheeseman, J. R., Scalmani, G., Barone, V., Petersson, G. A., Nakatsuji, H., Li, X., Caricato, M., Marenich, A. V., Bloino, J., Janesko, B. G., Gomperts, R., Mennucci, B., Hratchian, H. P., Ortiz, J. V., Izmaylov, A. F., Sonnenberg, J. L., Williams-Young, D., Ding, F., Lipparini, F., Egidi, F., Goings, J., Peng, B., Petrone, A., Henderson, T., Ranasinghe, D., Zakrzewski, V. G., Gao, J., Rega, N., Zheng, G., Liang, W., Hada, M., Ehara, M., Toyota, K., Fukuda, R., Hasegawa, J., Ishida, M., Nakajima, T., Honda, Y., Kitao, O., Nakai, H., Vreven, T., Throssell, K., Montgomery, J. A. Jr., Peralta, J. E., Ogliaro, F., Bearpark, M. J., Heyd, J. J., Brothers, E. N., Kudin, K. N., Staroverov, V. N., Keith, T. A., Kobayashi, R., Normand, J., Raghavachari, K., Rendell, A. P., Burant, J. C., Iyengar, S. S., Tomasi, J., Cossi, M., Millam, J. M., Klene, M., Adamo, C., Cammi, R., Ochterski, J. W., Martin, R. L., Morokuma, K., Farkas, O., Foresman, J. B. & Fox, D. J. *Gaussian 16* Revision C.01 (Gaussian Inc., Wallingford CT, 2016).
[68] U. Essmann, L. Perera, M. L. Berkowitz, T. Darden, H. Lee, L. G. Pedersen, "A smooth particle mesh Ewald method" *J. Chem. Phys.* **1995**, *103*, 8577–8593.
[69] D. A. Case, H. M. Aktulga, K. Belfon, D. S. Cerutti, G. A. Cisneros, V. W. D. Cruzeiro, N. Forouzesh, T. J. Giese, A. W. Götz, H. Gohlke, S. Izadi, K. Kasavajhala, M. C. Kaymak, E. King, T. Kurtzman, T. S. Lee, P. Li, J. Liu, T. Luchko, R. Luo, M. Manathunga, M. R. Machado, H. M. Nguyen, K. A. O'Hearn, A. V. Onufriev, F. Pan, S. Pantano, R. Qi, A. Rahnamoun, A. Risheh, S. Schott-Verdugo, A. Shajan, J. Swails, J. Wang, H. Wei, X. Wu, Y. Wu, S. Zhang, S. Zhao, Q. Zhu, T. E. Cheatham, D. R. Roe, A. Roitberg, C. Simmerling, D. M. York, M. C. Nagan, K. M. Merz, "AmberTools" *J. Chem. Inf. Model.* **2023**, *63*, 6183–6191.
[70] G. McLachlan, D. Peel, *Finite Mixture Models*, Wiley, **2000**.
[71] *Density Estimation for Statistics and Data Analysis*, Springer Netherlands, **1986**.
[72] J. A. Hartigan, P. M. Hartigan, "The Dip Test of Unimodality" *The Annals of Statistics* **1985**, *13*, DOI 10.1214/aos/1176346577.
[73] G. Žoldák, M. Rief, "Force as a single molecule probe of multidimensional protein energy landscapes" *Curr. Opin. Struct. Biol.* **2013**, *23*, 48–57.

Entry for the Table of Contents

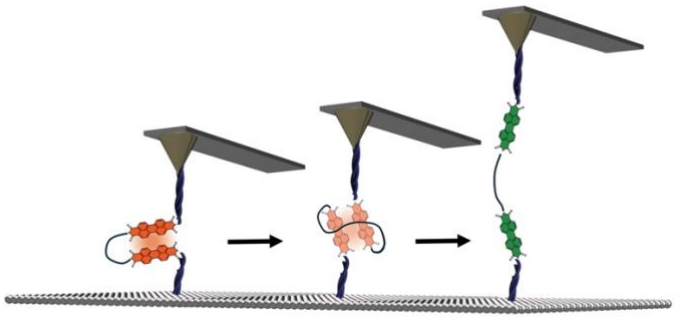

Mechanical force is used to probe π–π interactions within individual perylene diimide dimers by AFM-based force spectroscopy. Experiments and molecular dynamics simulations reveal two long-lived conformers with distinct mechanical stability and rupture pathways. Passive force spectroscopy quantifies their lifetimes under load and capture their dissociation pathways, providing insight into the energy landscape of noncovalent assemblies.